

Failure Characterization of Multi-Alloy and Multi-Gauge Hot-Stamped Tailor-Welded Blanks

Pedram Samadian^{1*}, Mary A Wells¹ and Michael J Worswick¹

¹ University of Waterloo, Department of Mechanical and Mechatronics Engineering,
200 University Avenue West, N2L 3G1, Waterloo, Ontario, Canada

* pedram.samadian@uwaterloo.ca

Abstract. To increase the ductility of hot-stamped structural components, the use of tailor-welded blanks (TWBs) of both high-strength and ductile steels has recently drawn attention. In this study, the failure behavior of the hot-stamped tailor-welded blanks (TWBs) comprising steel sheets of Ductibor®500-AS laser-welded to Usibor®1500-AS was investigated. TWBs with different combinations of 1.2 mm- and 1.6 mm-thick parent metals were hot-stamped and then tested under uniaxial-tension and equi-biaxial-tension loading conditions. Under longitudinal uniaxial-tension loading, all of the TWB types failed in the Usibor®1500-AS whereas in transverse uniaxial-tension loading, the failure occurred in the Ductibor®500-AS. Furthermore, in the equi-biaxial-tension tests, the 1.2 mm-1.6 mm TWBs presented the highest strains prior to failure, while fracturing in the Ductibor®500-AS sheet.

1. Introduction

The use of the hot stamping process for the fabrication of various vehicle parts has dramatically increased due to its remarkable opportunity for weight reduction and good crash performance [1]. In this process, steel sheets are heated to above the austenitization temperature for a given time and then simultaneously deformed and quenched in a die [2]. During such thermomechanical processing, components with very high strength are achieved due to martensitic transformation, which enables the possibility of the application of thinner sheets in a car body [3]. Therefore, besides higher safety, considerable cost savings are realized in terms of lower fuel consumption due to lower weight [4]. However, the high-intrusion resistance (high strength) of such hot-stamped material conditions does not result in a material condition suitable for energy absorption applications, as in front or rear rails, for example, since the fully martensitic material lacks sufficient ductility [5], [6]. To extend the application of hot-stamped steels, so-called *tailored-hot-stamping processes* have been developed in which the final component exhibits graded properties with a wide range of ductility and strength. One form of tailored hot stamping is through the use of tailor-welded blanks (TWBs) in which different steel sheets with specific chemical compositions and hardenability are first welded to each other and then hot-stamped. The difference in the hardenability of the steels results in different phase transformations so that one region attains a fully-martensitic microstructure whilst the other exhibits a multi-phase microstructure, usually martensite together with a softer phase such as bainite or ferrite [7]. This study examines a relatively new steel, known as Ductibor®500-AS, for use in the tailored hot stamping of TWBs comprising the Usibor®1500-AS laser-welded to the Ductibor® 500. Investigations have shown that after the hot stamping process, the tensile strength and elongation of the Usibor®1500-AS steel is around 1500 MPa and 6%, respectively, while the Ductibor®500-AS



exhibits about 550 MPa and 20%, respectively. Hence, the hot-stamped Ductibor®500-AS-Usibor®1500-AS TWBs can be applied in multi-function components that combine intrusion resistance and energy absorption [8], [9], for example.

In this study, the failure response of as-quenched laser-welded blanks comprising Ductibor®500-AS and Usibor®1500-AS was examined. For this purpose, longitudinal and transverse uniaxial-tension tests, in which the weld-line orientation is either parallel or perpendicular to the axial-loading direction, respectively, as well as equi-biaxial-tension dome tests were conducted on the TWBs, and the fracture locations and strains prior to failure were characterized. Mono-gauge TWBs were considered, with thicknesses of 1.2 or 1.6 mm, as well as multi-gauge TWBs comprising the 1.2 mm Ductibor®500-AS welded to the 1.6 mm Usibor®1500-AS.

2. Experiments

The material considered in this study consisted of 1.2 mm-1.2 mm-, 1.2 mm-1.6 mm-, and 1.6 mm-1.6 mm-thick laser-welded blanks of the Ductibor®500-AS and Usibor®1500-AS steel sheets, supplied by ArcelorMittal. The weld line was perpendicular to the rolling direction of the base metals, and the width of the weld zone was around 2 mm. The TWBs were first austenitized at 930 °C for 6.5 min and then die-quenched by means of a 900-ton hydraulic forming press. Next, the microstructures of the as-received and hot-stamped specimens across the weld line were investigated using light optical microscope (LOM). Standard JIS Z2201 No. 5 uniaxial tension specimens [10] with either longitudinal or transverse orientations of the weld line with respect to the loading direction were tested. In addition, 203.2 mm by 203.2 mm square samples for Nakazima dome tests were cut from the hot-stamped samples with the weld line in the middle of the specimens. These samples are referred to as “equi-biaxial” since their dimensions correspond to the so-called equi-biaxial geometry normally used for monolithic sheet samples; however, it is recognized that the differences in alloy and thickness within the TWB will affect the actual strain state. The tensile tests were performed using a 100 kN Instron servo-hydraulic machine with a strain rate of 0.01 s⁻¹, while the dome tests were carried out using an MTS-dome-tester apparatus with a 101.6 mm-diameter hemispherical punch, a punch speed of 0.25 mm/s, and binder force of 660 kN. The binder and die were equipped with male and female lock beads, respectively. The samples were located in the tooling such that the axis of the punch is aligned with the centre of the blank (and weld line). To decrease friction with the punch and obtain a fracture closer to the top of the dome, three sheets of Teflon coated with petroleum jelly were applied between the punch and samples. The number of repeat tests was at least 4 for each testing type. For all of the tests, in order to measure strain distribution, three-dimensional digital image correlation (DIC) techniques were utilized with Point Grey Research GRAS-50S5M-C cameras capturing the area of interest. To avoid the problem of paint flaking-off due to the separation of the Al/Si coating of parent metals during the tests, all samples were sandblasted in advance of testing to remove the coating. The DIC settings were adjusted such that local strain determination corresponded to a virtual strain gauge length (VSGL) [11] of 0.3 mm for all of the DIC analyses. The engineering or “nominal” strains from the tensile samples were determined using the average displacements from three 50 mm virtual, vertical extensometers drawn in the Vic-3D DIC software. To characterize the strain distribution across/along the parent materials, a line slice perpendicular to the weld line, passing through the fracture points, was plotted on the uniaxial-tension and dome specimens in Vic-3D. The major and minor surface strains at the fracture location of the dome samples were derived from a 0.5 mm-radius circular sampling area of interest. It should be noted that because the detection of a crack at the onset of fracture is visually challenging, the measured strain distributions from the dome tests are reported up to the image corresponding to maximum load, whereas the strain distributions in the tensile samples correspond to the image just prior to the visual observation of material separation. It is noted that these strain levels will represent lower bounds to the local fracture strains.

3. Results and Discussion

The microstructures of the as-received and hot-stamped TWBs are illustrated in Figures 1 and 2, respectively. Investigations showed that in the as-received condition, both Ductibor®500-AS and Usibor®1500-AS have ferritic-pearlitic microstructures, while the weld line centre is fully martensitic.

In the die-quenched condition, the Usibor®1500-AS and weld microstructures are martensitic whereas the microstructure of the Ductibor®500-AS consists of ferrite and martensite.

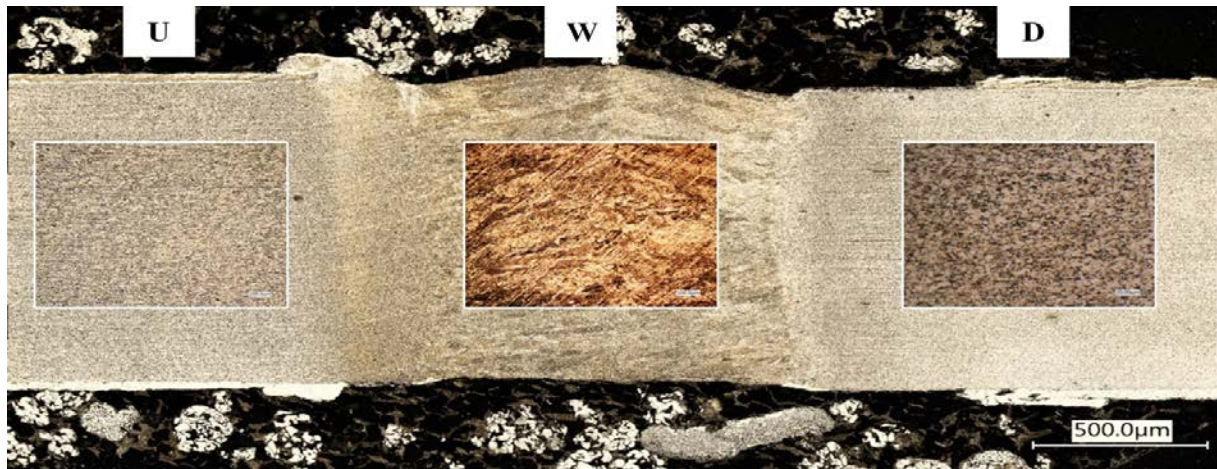


Figure 1. The LOM images of the microstructures of the as-received 1.2 mm-1.2 mm TWB across the weld line (U=Usibor®1500-AS, D=Ductibor®500-AS, and W=Weld).

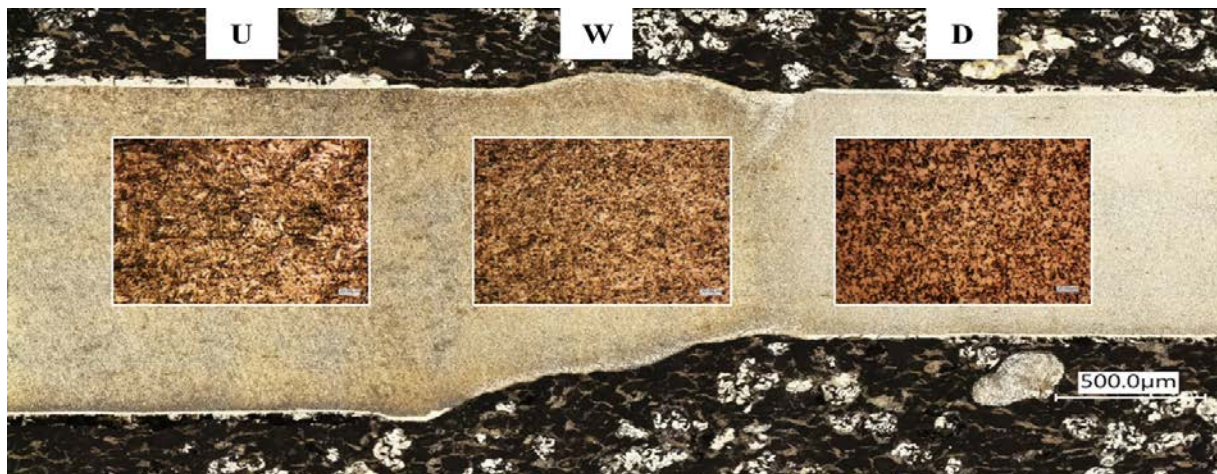


Figure 2. The LOM images of the microstructures of the hot-stamped 1.2 mm-1.6 mm TWB across the weld line.

Figure 3 shows the nominal axial stress-strain curves of the longitudinal tensile TWB samples up to the ultimate tensile strength (UTS) point, compared to those of the base metals (transverse direction (TD)). The nominal stress is taken as the tensile load divided by the nominal cross-sectional area of the TWB. The nominal stress at the UTS point and elongation to failure of the TWB samples are presented in Table 1.

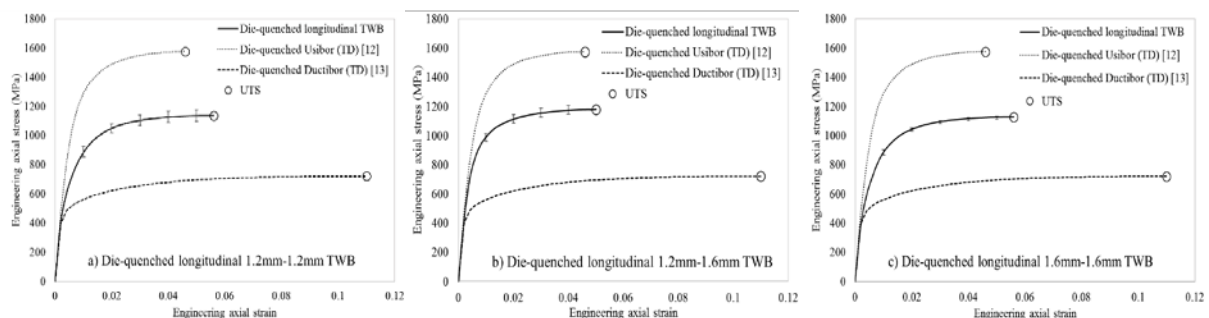


Figure 3. The averaged nominal axial stress-strain curves for the longitudinal tensile samples up to UTS; the a) 1.2 mm-1.2 mm, b) 1.2 mm-1.6 mm, and c) 1.6 mm-1.6 mm TWBs (Error bars correspond to the experimental scatter.).

Table 1. The UTS and maximum elongation of the longitudinal tensile TWB samples.

Material	UTS (MPa)	Elongation at failure (ef %)
Longitudinal 1.2 mm-1.2 mm TWB	1136 ($\sigma = 39^a$)	7.4 ($\sigma = 0.5$)
Longitudinal 1.2 mm-1.6 mm TWB	1179 ($\sigma = 22$)	7.5 ($\sigma = 0.4$)
Longitudinal 1.6 mm-1.6 mm TWB	1127 ($\sigma = 8$)	8.5 ($\sigma = 0.5$)

^a σ is standard deviation.

As can be seen, the longitudinal TWBs with various thicknesses have a very similar mechanical response. The 1.2 mm-1.2 mm and 1.2 mm-1.6 mm TWBs exhibit almost the same elongation to failure, while the 1.6 mm-1.6 mm TWB experienced around 13% more deformation before failure. Moreover, the longitudinal TWBs show intermediate deformation behavior in comparison with that of the base metals. One interesting point is that in all of the longitudinal TWBs, in which the weld line is parallel to applied force, fracture is initiated in Usibor®1500-AS. This behavior can be attributed to the fact that Usibor®1500-AS is the least ductile part of the weldment since, during the longitudinal tests, both alloys and the weld underwent the same amount of elongation prior to localization; hence, it is expected that the section with the lower ductility fails first. Figures 4 and 5 show the major and minor surface-strain distributions across the weld line at several levels of total deformation (indicated as a percentage of the failure elongation (ef)) and illustrate the manner in which the onset of final fracture occurs within Usibor®1500-AS. Both the major and minor strains are uniformly distributed across the weld line until almost 75% of the total elongation (ef). After that, strain localizes somewhere in the Usibor®1500-AS side, due to its lower ductility, and increases extensively until fracture (Figure 6a) whilst it does not change significantly in the other parts.

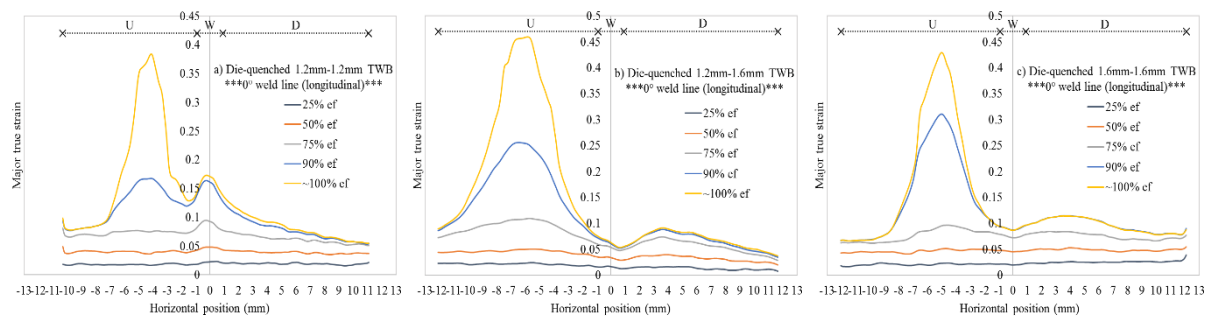


Figure 4. The major surface strain distribution across the weld line of the longitudinal tensile samples at several levels of total deformation; a) 1.2 mm-1.2 mm, b) 1.2 mm-1.6 mm, and c) 1.6 mm-1.6 mm.

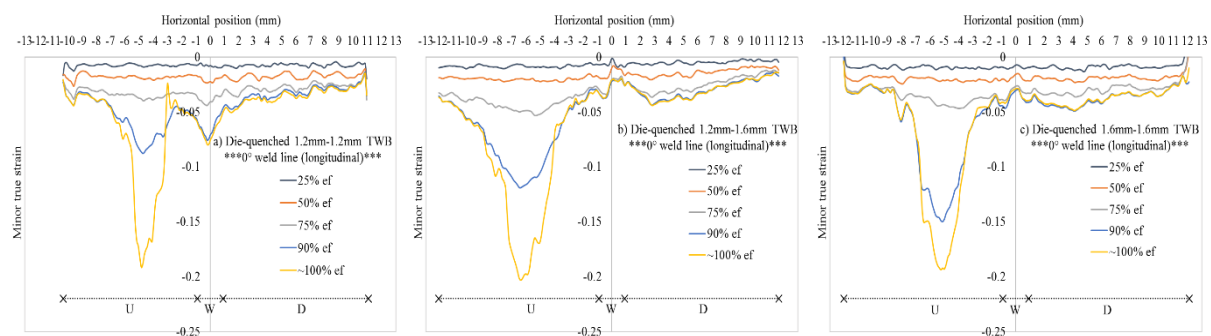


Figure 5. The minor surface strain distribution across the weld line of the longitudinal tensile samples at several levels of total deformation; a) 1.2 mm-1.2 mm, b) 1.2 mm-1.6 mm, and c) 1.6 mm-1.6 mm.

Figure 7 and Table 2 present the nominal axial stress-strain curves of the transverse tensile TWB samples, compared to those of the base metals (TD), and their UTS and maximum elongation, respectively. The results show that the 1.2 mm-1.6 mm TWB has a lower hardening rate than that of the 1.2 mm-1.2 mm and 1.6 mm-1.6 mm TWBs so that it displays around 10-15% lower strength at the maximum load. One possible source of this reduced load for the multi-gauge TWB under

transverse loading could be the induced bending caused by the offset of the centre plane of the two sheet materials at the weld. The total elongations of the transverse TWBs are comparable. Similar to the longitudinal TWBs, the transverse 1.6 mm-1.6 mm TWB has the highest total elongation. Interestingly, the UTS point of the transverse TWBs is close to that of Ductibor®500-AS, indicating that the load-carrying capacity is limited by the weaker base metal.

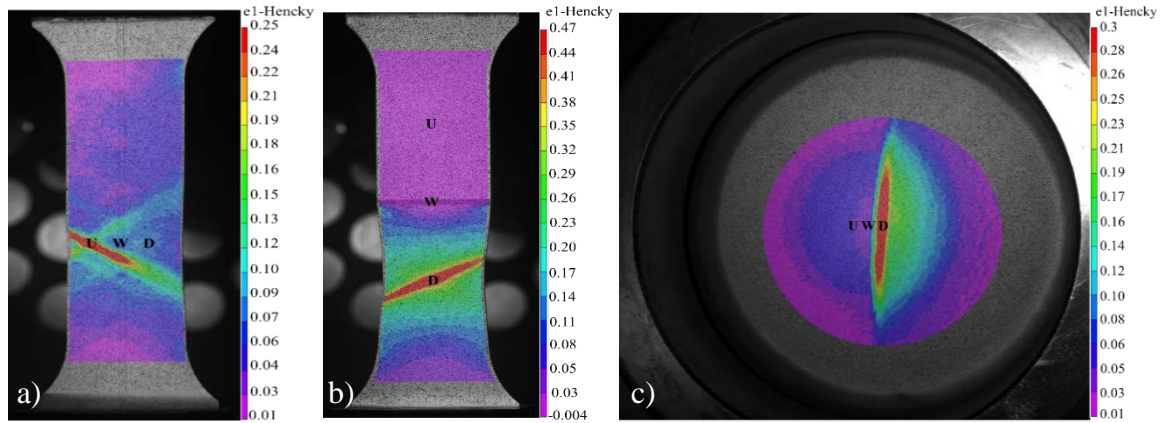


Figure 6. The major surface strain distribution at failure around the a) longitudinal tensile (1.2 mm-1.2 mm TWB), b) transverse tensile (1.2 mm-1.6 mm TWB), and c) equi-biaxial-tension (1.6 mm-1.6 mm TWB) samples.

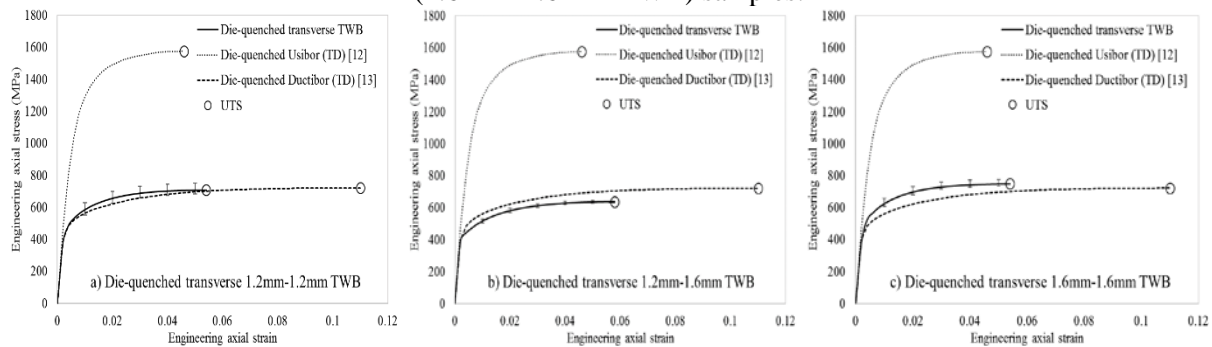


Figure 7. The averaged engineering axial stress-strain curves of the transverse tensile samples until the UTS point; a) 1.2 mm-1.2 mm, b) 1.2 mm-1.6 mm, and c) 1.6 mm-1.6 mm TWBs.

Table 2. The UTS and maximum elongation of the transverse tensile TWB samples.

Material	UTS (MPa)	Elongation at failure (ef %)
Transverse 1.2 mm-1.2 mm TWB	708 ($\sigma = 22^a$)	9.8 ($\sigma = 0.5$)
Transverse 1.2 mm-1.6 mm TWB	637 ($\sigma = 8$)	10.2 ($\sigma = 1.9$)
Transverse 1.6 mm-1.6 mm TWB	749 ($\sigma = 17$)	10.6 ($\sigma = 0.4$)

All of the transverse TWBs fractured in Ductibor®500-AS since deformation localizes in this region due to its lower strength. The major and minor surface strain distributions across the weld line of the transverse TWBs for various levels of total deformation are shown in Figures 8 and 9. Both figures demonstrate that from the initial stages of deformation, Ductibor®500-AS was the only region that underwent plastic deformation, and both Usibor®1500-AS and the weld line remained largely elastic. Strain localization in the Ductibor®500-AS is evident after 50% of the total elongation, resulting in the initiation of failure in this region (Figure 6b).

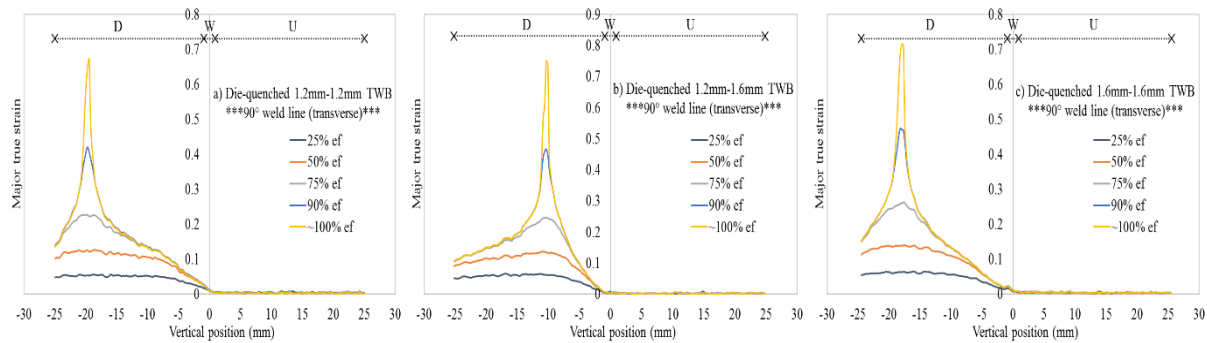


Figure 8. The major surface strain distribution across the weld line of the various transverse TWBs at several levels of total deformation; a) 1.2 mm-1.2 mm, b) 1.2 mm-1.6 mm, and c) 1.6 mm-1.6 mm.

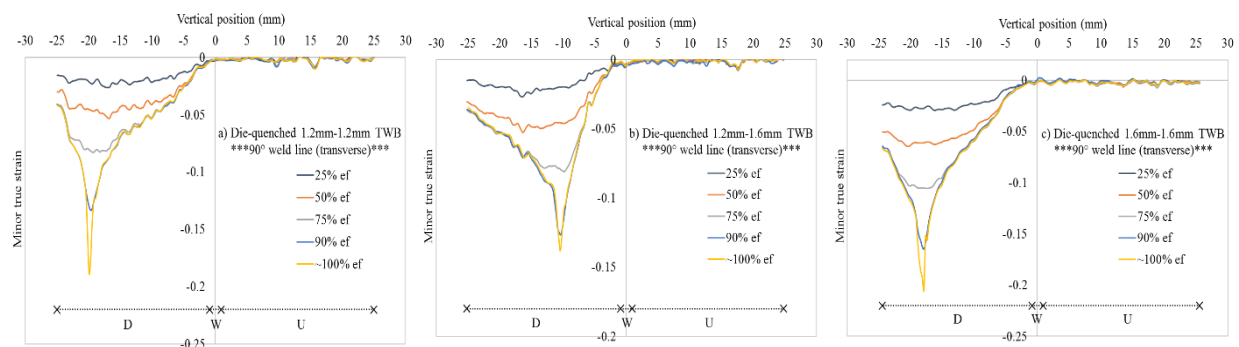


Figure 9. The minor surface strain distribution across the weld line of the various transverse TWBs at several levels of total deformation; a) 1.2 mm-1.2 mm, b) 1.2 mm-1.6 mm, and c) 1.6 mm-1.6 mm.

Figure 10 shows the punch load-displacement curves from the equi-biaxial-tension dome tests. Table 3 presents the average total punch displacement to failure as well as the equivalent strain at maximum load for the various TWBs.

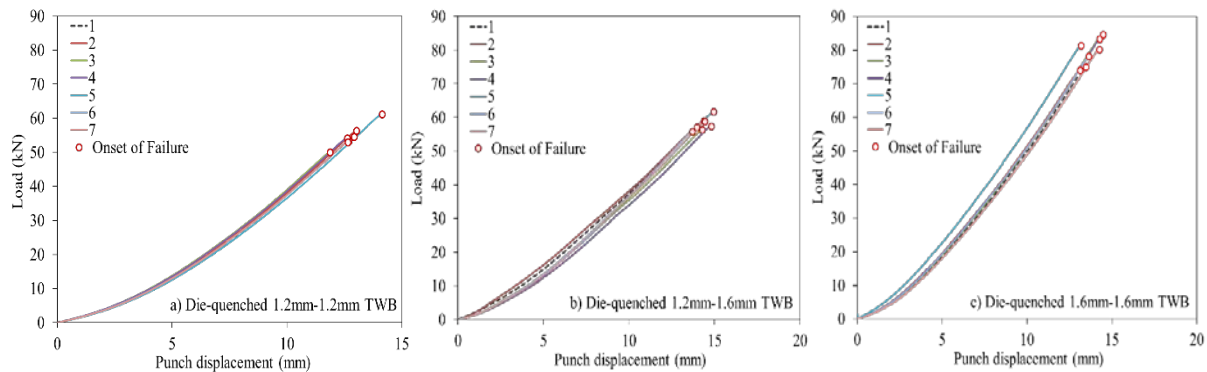


Figure 10. The punch load-displacement curves of the equi-biaxial-tension dome tests of the various TWBs; a) 1.2 mm-1.2 mm, b) 1.2 mm-1.6 mm, and c) 1.6 mm-1.6 mm.

Table 3. The average punch displacement and equivalent strain at maximum load for the various TWBs.

Material	Average punch displacement at maximum load (mm)	Average equivalent strain at maximum load
1.2 mm-1.2 mm TWB	12.85 ($\sigma = 0.68^a$)	0.43 ($\sigma = 0.02$)
1.2 mm-1.6 mm TWB	14.35 ($\sigma = 0.43$)	0.49 ($\sigma = 0.02$)
1.6 mm-1.6 mm TWB	13.77 ($\sigma = 0.56$)	0.44 ($\sigma = 0.03$)

As can be seen in Figure 10, the punch load-displacement curves of the different samples show reasonable repeatability for each TWB type. The punch load increases as the TWBs become thicker. Interestingly, the highest punch displacement and strain at failure are observed for the 1.2 mm-1.6 mm TWBs, and those of 1.2 mm-1.2 mm and 1.6 mm-1.6 mm TWBs are close (Table 3). All of the samples fractured in the Ductibor®500-AS sheet close to the weld (Figure 6c). Figure 11 depicts the distributions of major surface strains across the weld line in the different TWBs. The strain in the Ductibor®500-AS is higher than that seen in the weld and the Usibor®1500-AS. It is interesting to note that the plastic strain in Usibor®1500-AS is non-zero (unlike the transverse tensile samples in Figure 8) due to the deformation imposed by the punch geometry. Localization in the Ductibor®500-AS commences after about 25% of the failure strain. The fracture location in the multi-gauge TWB occurs further away from the weld, possibly due to the bending effect associated with the offset of the centre plane of the two sheets.

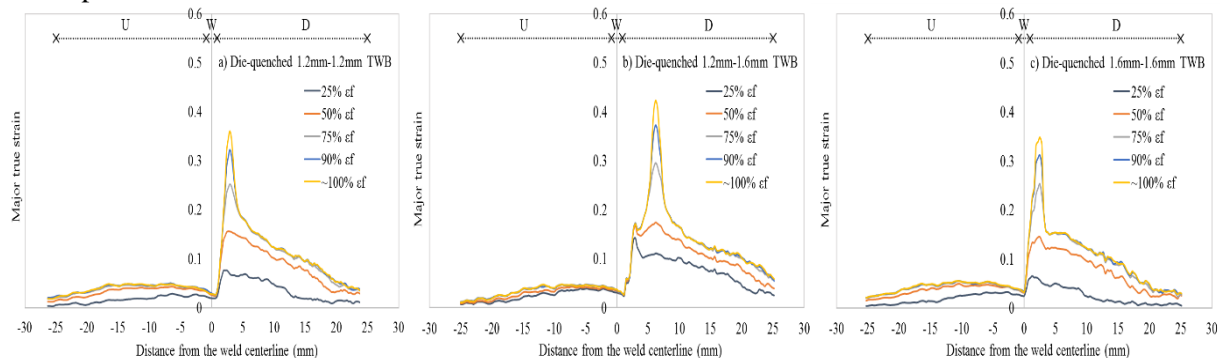


Figure 11. The major surface strain distribution across the weld line of the various TWB dome samples at several levels of total (failure) strain (ϵ_f); a) 1.2 mm-1.2 mm, b) 1.2 mm-1.6 mm, and c) 1.6 mm-1.6 mm.

Figure 12 shows the major versus minor strain paths at the fracture points of the different TWBs during the dome tests. The minor strains are initially positive during the early stages of deformation; this effect is associated with the biaxial bending as the sheet engages the spherical punch. It is interesting to note that the balance of the deformation occurs under an incremental plane-strain-tension condition despite the blank geometry corresponding to that used for an equi-biaxial-tension test, at least for monolithic (non-TWB) blanks. The prevalence of the plane-strain condition can be attributed to the higher strength (and thickness for the multi-gauge TWB) of Usibor®1500-AS which constrained the lateral expansion of Ductibor®500-AS along the weld line.

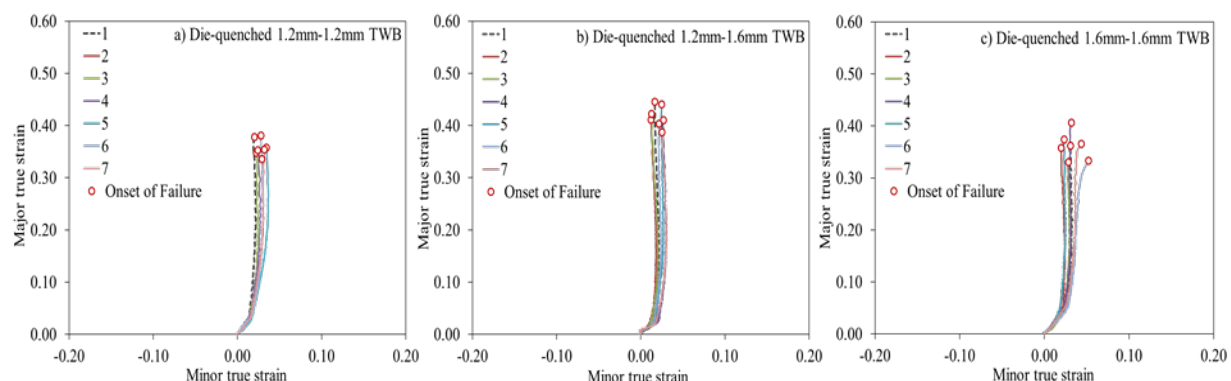


Figure 12. The major versus minor surface strain paths at the fracture points of the different TWBs during the dome tests; a) 1.2 mm-1.2 mm, b) 1.2 mm-1.6 mm, and c) 1.6 mm-1.6 mm.

4. Conclusion

This paper has served to provide an initial characterization of the failure behavior of hot-stamped TWBs of Ductibor®500-AS and Usibor®1500-AS. For the transverse uniaxial-tension and equi-biaxial-tension samples, strain (and failure) is concentrated in the lower strength Ductibor®500-AS. In

contrast, failure occurs in the less ductile Usibor®1500-AS for the longitudinal uniaxial-tension test. Of particular interest in the dome-tests was the constraint effect of the higher strength Usibor®1500-AS side which forced the Ductibor®500-AS side of the weld to experience a predominantly plane-strain state.

Acknowledgments

Support for this research from Honda R&D Americas, Promatek Research Centre (Cosma International), ArcelorMittal, Automotive Partnerships Canada, the Natural Sciences and Engineering Research Council, the Ontario Research Fund, and the Canada Research Chairs Secretariat is gratefully acknowledged.

References

- [1] Karbasian H and Tekkaya A E 2010 A review on hot stamping *J. Mater. Process. Technol.* **210** (15) 2103-18
- [2] K. Omer *et al.* 2017 testing of a hot stamped axial crush member with tailored properties – experiments and models *Int. J. Impact Eng.* **103** 12-28
- [3] Naderi *et al.* 2011 Semi-hot stamping as an improved process of hot stamping *J. Mater. Sci. Technol.* **27** (4) 369-376
- [4] Li N 2013 *Fundamentals of Materials Modelling for Hot Stamping of UHSS Panels with Graded Properties* (Imperial College London)
- [5] Bardelcik A 2013 High Strain Rate Behaviour of Hot Formed Boron Steel with Tailored Properties (University of Waterloo)
- [6] Bois P D *et al.* 2004 *Vehicle Crashworthiness and Occupant Protection* (American Iron and Steel Institute)
- [7] Prajogo Y 2015 Hot Stamping of a Boron Steel Side Impact Beam with Tailored Flange Properties - Experiments and Numerical Simulations (University of Waterloo)
- [8] 2008 *Steels for Hot Stamping* (ArcelorMittal)
- [9] 2017 *Steels for Hot Stamping -Usibor® and Ductibor®* (ArcelorMittal)
- [10] Sulamet-Ariobimo R D *et al.* 2016 Tensile properties analysis of AA1100 aluminium and SS400 steel using different JIS tensile standard specimen *Rev. Mex. Trastor. Aliment.* **14** (2) 148-153
- [11] Rahmaan T *et al.* 2017 Investigation into the shear stress, localization and fracture behaviour of DP600 and AA5182-O sheet metal alloys under elevated strain rates *Int. J. Impact Eng.*, **108** 303-321
- [12] Ten Kortenaar L 2016 Failure characterization of Hot Formed Boron Steels with Tailored Mechanical Properties (University of Waterloo)
- [13] Samadian P *et al.* *Constitutive Modelling of the Flow Behavior of the Different Microstructures of Ductibor®500 Steel* Conf. 2nd ICILSM May 2018 Xi'an China